



ICEE 2016 Okinawa

The International Conference on Electrical Engineering 2016
3 - 7 July 2016, Okinawa Jichikaikan, Okinawa, Japan



一般社団法人電気学会
The Institute of Electrical Engineers of Japan



HKIE

The theme of ICEE 2016 is "Future Technology for Bridging Nations"

Welcome Message

Committee

Full Paper

ACKNOWLEDGEMENTS

Organized by:

The Institute of Electrical Engineers of Japan (IEEJ)

Co-organized by:

The Chinese Society for Electrical Engineering (CSEE)

The Hong Kong Institution of Engineers (HKIE)

The Korean Institute of Electrical Engineers (KIEE)

This conference is supported by JSPS KAKENHI Grant No. 15HP0702.

Session D1-8 : 5-01 Diagnosis and Sensing Systems, 5-05 Other Related Areas

Day 3 (July 6) 10:50-12:50 Room D1

90007

Takashi Takiya, Tsuyoshi Uchiyama

Common-Mode Magnetic Field Rejection-type MI Gradiometer

90073

Takafumi Komuro, Takahiro Hoshino, Kazuhiro Tsuboi, Yoshio Hamamatsu

A Merging Control Strategy with a Waiting Time Limit in a Personal Rapid Transit System

90115

Iida Mirai, Iliana Marinova, Saito Yoshifuru

Geomagnetic fields analysis by the generalized frequency fluctuation method

90153

Takahiro HYUGA, Naoto ISHIKAWA, Iliana MARINOVA, Yoshifuru SAITO, Manabu OHUCHI, Takaharu KOJIMA

Enhance the Sensibility of the film infinite Eddy Current Sensors

90185

Kazuya Okuda, Yoshifuru Saito, Iliana Marinova

Ingenious Resonance Circuit Connection for Resonance Type Eddy Current Sensors

90512

Suttipong Boontaklang, Chai Chompoo-inwai, Rujira Lakatem, Siriwat Potivejakul, Chow Chompoo-inwai

Novel Automatic Resonance Frequency Tracking Method for 1 MHz Ultrasonic Piezoelectric Transducers Using dsPIC-Microcontroller and PLL Technique

90515

Rujira Lakatem, Monthon Leelajindakraierk, Siriwat Potivejakul, Chow Chompoo-inwai

The conceptual design and a partial development of a multi-function therapeutic stimulator

Generalized frequency fluctuation analysis of the geomagnetic fields

Mirai IIDA and Yoshifuru SAITO
 Electrical and Electronic Engineering, Hosei University
 Y.Saito Lab, 3-7-2 Kajino
 Koganei, Tokyo 184-8584, Japan

Iliana MARINOVA
 Technical University of Sofia 1756, Sofia, Bulgaria

Abstract

A big earthquake on March 11th 2011 occurred at the eastern side of Japan caused serious damages to the human life and the modern infrastructures. We try to evaluate a relationship between the earthquake and geomagnetic fields by means of the generalized frequency fluctuation analysis. The n^{th} order fluctuation analysis methodology is one of the generalizations of the 1st order fluctuation analysis, i.e., the 1/f frequency fluctuation.

Keywords: Geomagnetic fields, Frequency fluctuation, Least squares.

1 INTRODUCTION

As is well known, most of the recent major disasters had been caused by the natural earthquakes. In particular, a big natural earthquake on March 11th 2011 occurred at the eastern side of Japan caused serious damages to the human life and the modern infrastructures. Forecast of the big earthquake is of paramount importance to protect not only our human life but also modern infrastructures. Even though the intensive investigations to forecast the time and location of the big earthquake have been carried out and continued until now mainly by the seismologists, it is still difficult to obtain the satisfactory forecast accuracy in order to avoid the major disasters [1].

In the present paper, we try to evaluate a relationship between the earthquake and geomagnetic fields by means of the earth magnetisms. More precisely, we try to evaluate the relationship between the earthquake and geomagnetic fields by means of the generalized frequency fluctuation analysis.

Well known frequency fluctuation is the 1/f fluctuations observed in many natural phenomena such as the sound caused by natural wind, illuminating strength by fireflies and so on [2]. Also, the other well known fact is that the 1/f fluctuations may give the healing and relaxation effects to the human beings.

Previously, we have elucidated that application of the 1/f fluctuation analysis to the Barkhausen signals accompanying with the magnetization of ferromagnetic materials reveals the stress situations of the ferromagnetic materials [3-6].

One of the drawbacks of our developed frequency fluctuation

approach is to require human skill to decide the frequency range to be analyzed [2]. The principal purpose of this paper is to remove this drawback from our generalized frequency fluctuation method.

Our frequency fluctuation method is a generalization of the well-known 1/f fluctuation analysis. Conventional 1/f frequency fluctuation analysis employs a simple straight line decided by the least squares in the both logarithmic frequency and Fourier power spectrum space [2]. In addition, we have generalized the 1/f fluctuation analysis to a more sophisticated n^{th} order fluctuation analysis methodology [3-6].

The n^{th} order fluctuation analysis methodology is that the 1st order least squares approximation line is generalized to the n^{th} order least squares approximation curves to represent the frequency characteristic in the both logarithmic frequency and Fourier power spectrum space, i.e., a straight line approximation is generalized to the n^{th} order approximate curves a_0+a_1f to $a_0+a_1f+a_2f^2+\dots$ in the both logarithmic frequency and Fourier power spectrum space, where a_0, a_1, a_2 and f are the 0th, 1st, 2nd order coefficients and frequency, respectively.

2 FREQUENCY FLUCTUATION ANALYSIS

2.1 1/f frequency fluctuation

One of the most famous frequency fluctuations is the 1/f frequency fluctuation, which can be observed in most of the natural phenomena such as natural wind, sea tide water waves,

sound accompanying river flows and so on, giving a healing effect to the mentalities via human sensibilities [2].

Conventional $1/f$ frequency analysis is that application of the 1^{st} order least squares fit to the both Fourier power spectrum and frequency extracts the 1^{st} order frequency fluctuation, i.e., Fourier power spectrum is approximated by $a_0 + a_1 f$, yields a 1^{st} order frequency fluctuation characteristic in the both logarithmic frequency and Fourier power spectrum space, where a_0 and a_1 are the 0^{th} and a 1^{st} order frequency fluctuation terms, respectively. If the frequency fluctuation term a_1 takes $a_1=-1$, then we have the $1/f$ frequency fluctuation.

When 1^{st} order frequency fluctuation term takes zero, Fourier power spectrum becomes a constant value regardless frequency as shown by a dotted line in Fig. 1. This type of signal is called the white noise, and gives uncomfortable feeling to the human because of the too heavy randomness.

On the other side, regular signal, e.g., $a_1=-2$ leading $1/f^2$ shown by a steep line in Fig.1, gives also uncomfortable feeling because of the too fixed regularity.

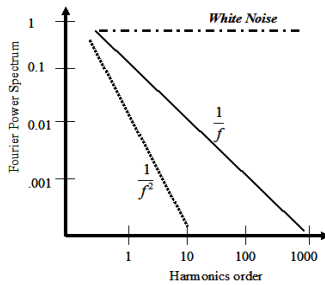


Figure 1. 1^{st} order frequency fluctuation

Thus, a signal located at the midway between the complete random and regular signals, i.e., $a_1=-1$ in Fig. 1, is called the $1/f$ frequency fluctuation. This gives a comfortable feeling to the human mentalities. Probably a reason why $1/f$ frequency fluctuation signal gives the gentle and comfortable feeling to the human sensibilities is that the $1/f$ frequency fluctuation signal may be included in the most of the natural phenomena [2].

2.2 Generalization of the frequency fluctuation

Let us consider the both logarithmic frequency and Fourier power spectrum space hereafter the dissections. When we apply the 1^{st} order frequency fluctuation fit to the earth magnetism signal, it is obviously difficult to extract the essential characteristics of the earth magnetism signal due to its intrinsic randomness. To overcome this difficulty, we employ a higher order curve given by a power series of (1) instead of a simple line $a_0 + a_1 f$.

$$h(f) = a_0 + a_1 f + a_2 f^2 + \dots + a_n f^n \quad (1)$$

The coefficients $a_0, a_1, a_2, \dots, a_n$ which construct a $n+1$

order vector \mathbf{A} in (2) are determined by the least squares. Further, if we are given the $m+1$ Fourier power spectra, i.e., $h(y_0), h(y_1), h(y_2), \dots, h(y_m)$, then it is possible to compose the vector \mathbf{Y} as (4), then a $m+1$ by $n+1$ rectangular matrix C (3) could be derived from the assumed higher order power series function (1).

$$\mathbf{A} = \begin{bmatrix} a_0 \\ a_1 \\ \vdots \\ a_n \end{bmatrix} \quad (2)$$

$$C = \begin{bmatrix} 1 & f_0 & f_0^2 & \dots & f_0^n \\ 1 & f_1 & f_1^2 & \dots & f_1^n \\ 1 & f_2 & f_2^2 & \dots & f_2^n \\ \vdots & \vdots & \vdots & \ddots & \vdots \\ 1 & f_m & f_m^2 & \dots & f_m^n \end{bmatrix} \quad (3)$$

$$\mathbf{Y} = \begin{bmatrix} h(y_0) \\ h(y_1) \\ \vdots \\ h(y_m) \end{bmatrix} \quad (4)$$

Since a condition $m \gg n$ is satisfied, then the least squares could be applicable. Hence, the vector \mathbf{A} whose elements are the $a_0, a_1, a_2, \dots, a_n$ is evaluated by (5) [3-6].

$$\mathbf{A} = [C^T C]^{-1} C^T \mathbf{Y} \quad (5)$$

Figure 2 shows the typical signal and the 5^{th} order curve which are the thin lines and the thick lines, respectively.

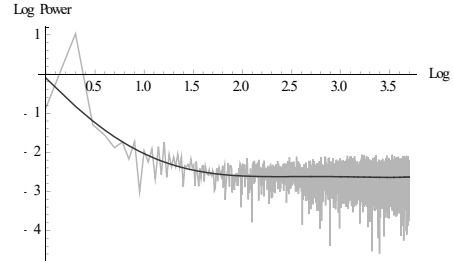


Figure 2. Typical frequency characteristic of the signal drawn by the thin lines and its 5^{th} order least squares curve drawn by the thick line.

2.3 Frequency fluctuation analysis of the geomagnetism

We apply the generalized frequency fluctuation analysis to geomagnetism data. The geomagnetic field data are defined in a vector field, and are represented by the three-dimensional vector quantities [7]. The independent three elements H,D,I are the geomagnetic fields in a certain observation point. The other factors are evaluated from three elements by (6).

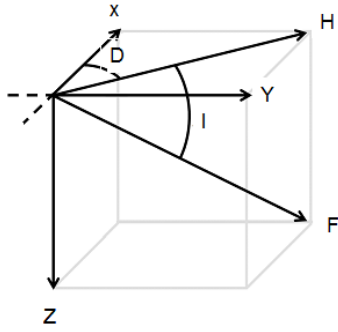


Figure 3. Geomagnetic field resolution elements

$$\begin{aligned}
 F &= \sqrt{X^2 + Y^2 + Z^2} = \sqrt{H^2 + Z^2} \\
 H &= F \cos(I) \\
 X &= H \cos(D) \\
 Y &= H \sin(D) \\
 Z &= F \sin(I)
 \end{aligned}
 \tag{6}$$

Table 1. Various constants of geomagnetic field elements

F	Total intensity	Magnitude of the geomagnetic field.
D	Declination	Deviation between the horizontal component H and northward component X.
I	Inclination	Deviation between the total intensity F and horizontal component H.
H	Horizontal component	Magnitude of the geomagnetic field in the horizontal plane.
Z	Vertical component	Magnitude of the geomagnetic field in the perpendicular direction to the earth surface.
X	Northward component	Magnitude of the geomagnetic field on North-South direction axis.
Y	Eastward component	Magnitude of the geomagnetism on East-West direction axis.

Independent three elements are the horizontal component H, declination D, and a vertical component Z. Otherwise; a combination of component X facing north, component Y facing east, vertical component Z are used. But total intensity F, inclination I, and declination D are used most. These are called three elements of the geomagnetic field. The dimension of magnetic flux density F is a T (Tesla). The geomagnetism is very small so that the dimension nT (nano Tesla) is commonly used. Also, the dimension of inclination I and declination D is minute unit.

The geomagnetic field is depending on time, and is caused by

a sunbeam being irradiated to the existing ionosphere between the magnetosphere and the atmosphere of the earth. Therefore the geomagnetic field has a change of 1 diurnal parallax depending on the rotation of the earth. We call this "daily fluctuations" of the geomagnetic field.

On the other hand, "geomagnetic secular variation" is the changes in the geomagnetic field on time scales of about a year or more. This geomagnetic secular variation, whose period is from the several decades to the several hundred years, is caused mainly by the interior of the earth.

For example, the declination D defined by the deviation between the geomagnetic and geographical north directions in Table 1 is approximately 7 degrees in Tokyo metropolitan area, and has been 0.7 degree changed during recent 40 years. The magnetic north component X almost is the same as those of approximately 200 years ago so that the declination D is one of the typical geomagnetic secular variations.

Since the geomagnetic secular variation is caused in the interior of earth, then our generalized frequency fluctuation analysis is applied to the declination D [7].

A thin line in Fig. 4 is an original frequency characteristic of a daily fluctuation for which the change of daily changes should be one of the components of geomagnetic secular variation. The frequency is divided into several frequency ranges 1-10, 10-100, 100-1000 and so on while the logarithm base has been taken to 10. Higher order approximates of (1) is applied to each of the divided frequency ranges. Further, the normalized coefficients a_0, a_1, a_2 in (1) are respectively taken to the x, y, z coordinate values of a three dimensional Cartesian coordinate system, i.e., the frequency fluctuation characteristics are visualized in the 3D space.

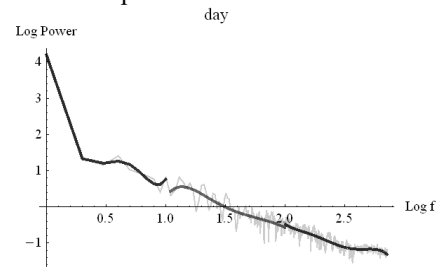


Figure 4. Typical frequency characteristic of a daily fluctuation whose frequency range is divided into the 1-10, 10-100, 100-1000 frequency ranges while the logarithm base has been taken to 10.

On March 11th 2011, Japan islands were shaken by a big earthquake whose magnitude is 9.0, and the epicenter is the Miyagi east southeast offing. The focal region was the extensive from the Iwate to the Ibaraki offing.

Seismic intensity recorded at Esashi observatory station is a little less than six. Also, seismic intensity recorded at Kanoyama observatory station is less than five on the earthquake disaster day. The Kanoyama observatory station is located at Kimitsushi in Chiba prefecture.

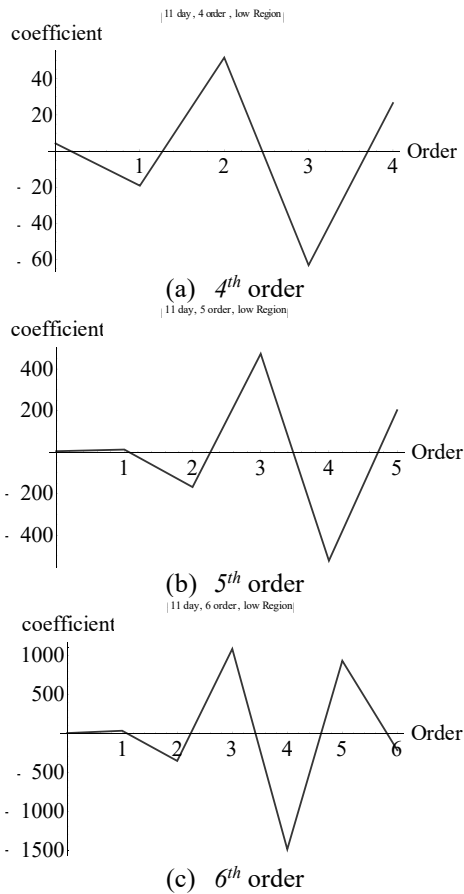


Figure 5. The values of coefficients $a_0, a_1, a_2, \dots, a_n$ when applying the curve of (1) to the first frequency 1-10 range in Fig. 4, where the order n has been changed from the 4th to 6th in (1).

Our generalized frequency fluctuation analysis has employed the declination D data recorded at the both Esashi and Kanoyama observatory stations.

Fig. 5 shows the values of coefficients $a_0, a_1, a_2, \dots, a_n$ when applying the curve of (1) to the first frequency 1-10 range in Fig. 4, where the order n has been changed from the 4th to 6th in (1). A target declination D data was recorded at the Kanoyama observatory station on March 11th 2011.

Let us consider the first three coefficients a_0, a_1, a_2 in Figs. 5(a)-5(c), then a second coefficient a_1 takes a negative value over the $n=5^{th}$ approximation curve while a_1 takes always positive value under the $n=5^{th}$ approximations.

Since the first three coefficients a_0, a_1, a_2 take the similar tendency as shown in the Figs. 5(b) and 5(c), then the $n=5^{th}$ order curve may be considered as the maximum order to represent the intrinsic frequency fluctuation characteristic of the first low frequency range in Fig. 4.

The first three coefficients a_0, a_1, a_2 are normalized to the a_0' ,

a_1', a_2' taking the values between the 0 to 1. Let us these normalized coefficients a_0', a_1', a_2' respectively be the x, y, z axis values, then it is possible to visualize the results of generalized frequency fluctuation analysis in a 3D space.

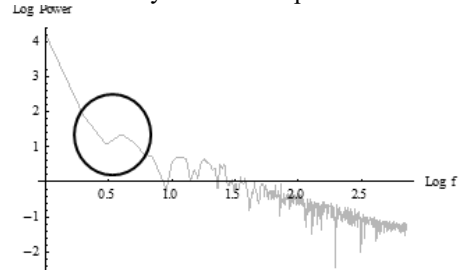


Figure 6. Extraction of the singular point of a big earthquake on March 11th 2011. A circle refers to the target frequency range for the frequency fluctuation analysis.

Thus, we applied our approach to the declination D data on March 11th 2011. Fig. 6 shows the frequency characteristic of the declination D data on March 11th 2011. A circle in Fig. 6 refers to a singular point of the frequency characteristic curve.

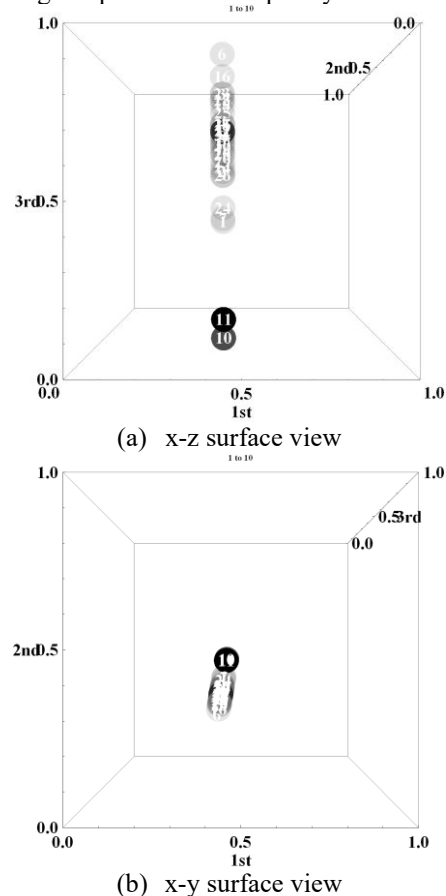


Figure 7. 3D visualization of the results when the generalized frequency fluctuation analysis is applied to the declination D data on March 11th 2011 recorded by Kanoyama observatory station.

Our generalized frequency fluctuation approach is applied to the low frequency range including the singular point in Fig. 6. Figs. 7 and 8 show the results of this analysis, where the thick solid dot denotes the point on March 11th 2011. The anterior and posterior days of this disaster day are denoted by the slightly thick solid dots in Figs. 7 and 8. Thus, we have succeeded in extracting the big earthquake day on March 11th 2011 among the one month 30 days declination D data.

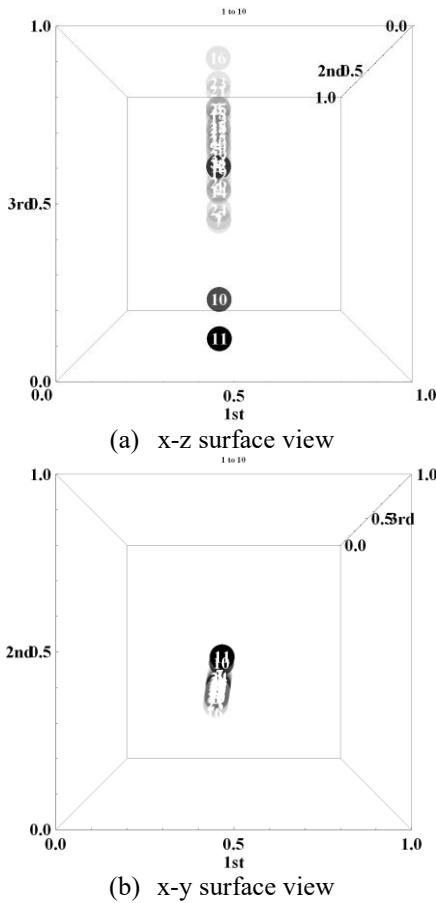


Figure 8. 3D visualization of the results when the generalized frequency fluctuation analysis is applied to the declination D data on March 11th 2011 recoded by Esashi observatory station.

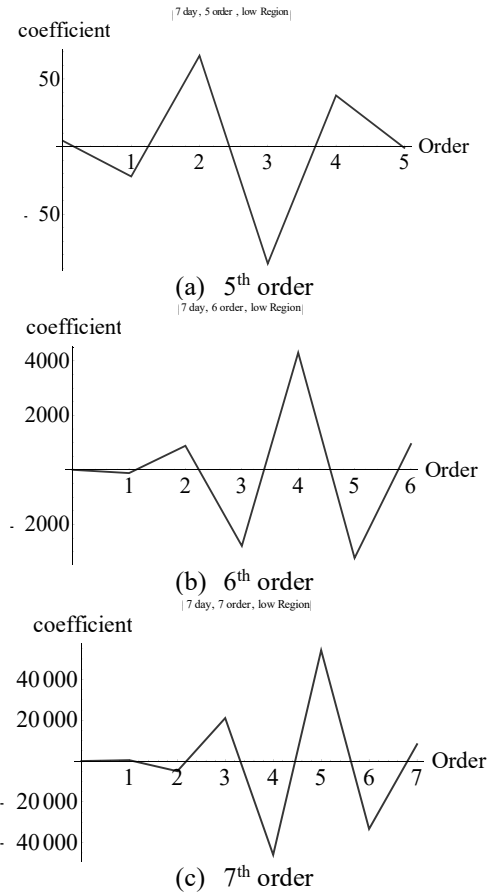
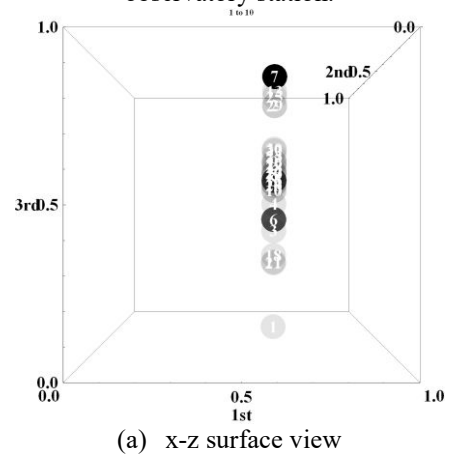
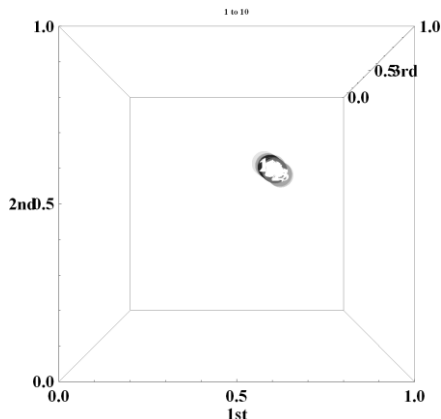


Figure 9. The values of coefficients $a_0, a_1, a_2, \dots, a_n$ when applying the curve of (1) to the first frequency 1-10 range of the daily variation on April 7th 2011 recoded by Esashi observatory station.





(b) x-y surface view

Figure 10. 3D visualization of the results when the generalized frequency fluctuation analysis is applied to the daily variation data recorded by Esashi observatory station on April 7th 2011.

To check the validity of our approach, we applied our approach to the daily variation on April 7th 2011 recorded by Esashi observatory station when observed a magnitude 6.6 earthquake at the Fukushima Hama Street.

Fig. 9 shows the value of coefficients $a_0, a_1, a_2, \dots, a_n$ when applying the curve of (1) to the first frequency 1-10 range of the declination D data on April 7th 2011, where the order n has been changed from the 5th to 7th in (1).

Similar to the previous one shown in Figs.5, we have employed the $n=6^{\text{th}}$ order approximation curve in (1) to extract the characteristics of April 7th among the 30 daily variation data on April in 2011.

Fig. 10 shows the results of our frequency fluctuation analysis, where the thick solid dot denotes the point on April 7th 2011. The x-z surface view in Fig. 10(a) succeeds to extract the April 7th, but the x-y surface view could not succeed to extract the April 7th because of overlapping the results.

As shown above, a big earthquake whose magnitude 9 is possible to extract the day occurred a big earthquake, and also possible to extract the day occurred 6.6 magnitude earthquake even though the anterior and posterior days could not be extracted.

3 CONCLUSIONS

The geomagnetic signals accompanying with the Great East Japan Earthquake have been analyzed by the generalized frequency fluctuation method. As a result, it has been clarified that the geomagnetic signals accompanying with the earthquakes always inform the some kind of physical signals concerning to the dynamics of earth.

A number of processed examples are too small to derive a deterministic conclusion.

A reliable result is that the geomagnetic field always includes the earthquake information. Thereby, it is possible to extract

the day occurred the earthquake among the 1 month 30 days daily variation data by means of the relevant signal processing Methodology.

A serious problem is to find the relevant signal processing methodology not depending on the expert skillfulness [3-6].

In the present paper, we have proposed one of the signal processing methodologies not depending on the human skill.

REFERENCES

- [1] The Coordinating Committee for Earthquake Prediction, Japan, <http://cais.gsi.go.jp/YOCHIREN/index.e.html>
- [2] T.Musha, S.Sato and Y.Yamamoto (Eds), "Noise in Physical Systems and 1/f Fluctuation", Amsterdam IOP Press, 1992.
- [3] S. Nojima and Y. Saito, "Application of frequency fluctuation to Barkhausen signals and its application", J. Magn. Soc. Japan, 2011, vol. 35, pp. 380-385,
- [4] Jun KAWAZOE, Iliana Marinova and Yoshifuru SAITO, "Fluctuation Frequency Analysis of the Barkhausen Signals", Proceedings of The 2012 Asia - Pacific Symposium on Applied Electromagnetics & Mechanics, pp.244-249.
- [5] J.Kawazoe and Y.Saito, "Analysis of Frequency Fluctuation Using Barkhausen Signal", J.Magn.Soc.Japan, 2013, vol.37, pp.320-326.
- [6] Jun Kawazoe, Iliana Marinova, Yoshifuru Saito, "Fluctuation Frequency Analysis of the Barkhausen Signals Under Static and Dynamic Stresses", IEEE Trans. Magnetics, vol.49, No.5, pp.1997-1999, May, 2013.
- [7] GSI Geomagnetic Survey, <https://geoinfo2.gsi.go.jp/contact/Inquiry2.aspx?pcode=1002&bcode=100202&mcodes=10020206>

Contact E-mail Address: mirai.iida.27@gmail.com

Enhance the Sensibility of the Film Infinite Eddy Current Sensors

Takahiro HYUGA, Naoto ISHIKAWA, Yoshifuru SAITO
Electrical and Electronics Engineering, Hosei University
Koganei Kajino, Tokyo 184-8584, Japan

Iliana MARINOVA
Technical University of Sofia
Sofia, 1756, Bulgaria

Manabu OHUCH, Takaharu KOJIMA
Denshijiki (Emic) Co. Ltd
Ukima 5-6-20, Kitaku, Tokyo 115-0051

Abstract

Previously, we have succeeded in exploiting a new high sensibility eddy current testing (ECT) sensor called the infinite coil. Operating principle of this infinite coil is that two adjacent coils constructing the north and south poles alternatively set a zero magnetic potential region and keep the same situation when eddy currents are flowing along the paths in parallel to the exciting coils. If the eddy currents could not flow the paths in parallel to the exciting coil on the test specimen, then a zero magnetic potential region between the two exciting coil moves toward the other position. This means that a sensing coil located at a mid position of two exciting coil is possible to detect the disturbed magnetic fields, i.e., the defect in the test specimen could be caught on the sensing coil signal.

In this paper, we have enhanced the sensibility of the infinite coil by increasing the no polarity zone between the north and south exciting poles. Employment of the two semicircular exciting coils has made it possible to enlarge the no polarity zone (viz., zero magnetic potential region). In addition, the results of the 3D finite element simulation and of the practical experiments have verified that the our new developed semicircular infinite coil is higher sensibility than those of conventional one.

Keywords: nondestructive testing, ECT, design practice, enhancement of sensor

1 INTRODUCTION

Most of the industrial products and infrastructures are composed of the mechanical frames, and they support our modern civilianized human life. Each of the machines is composed of the mechanical parts to support its mechanical strength as well as their shapes.

Major frame materials are the pure metallic or their compound, and are always stressed to maintain the highly civilized modern human life. The stress is classified into the mechanical, thermal and so on, which lead to the cause of fatigue and defect.

To keep the highest safety and reliability, various maintenance works to the machines as well as infrastructures are continuously required as one of the most important tasks. To evaluate the metal fatigue, one of the most fundamental and important methodologies is the nondestructive testing to the metallic materials [1].

The nondestructive testing makes it possible to evaluate the defect size, shape and situations without any destroying and decomposing the products. Further, we have several nondestructive methods such as the eddy current testing (ECT), electrical potential method, ultrasonic imaging, x-ray tomography and so on [2,3].

Among various nondestructive methodologies, the ultra sonic method is capable of highly reliable and precise results, but it is required the direct contact to the tested specimen. Also, nondestructive inspection by the electrical potential method requires direct contact to the target object. Radioactive method is limited in its use from the safety handling viewpoint.

On the other side, the ECT is composed of the relatively simple parts and needs not the direct contact to the tested specimen. Furthermore it is possible to operate in a relatively high speed, even though sometimes it is difficult to detect the defects in the target metallic object depending on the eddy current flowing paths. However, the ECT has versatile

capabilities as the nondestructive testing method.

The operating principle of the ECT is classified into two major categories. One is the impedance sensing type whose operating principle is that the ECT probe and target object are regarded as the primal and secondary circuits of a transformer, respectively. So that the change of secondary impedance caused by the defects could be detected from the primal input impedance change. One of the merits of the impedance sensing type is that this ECT is composed of the simplest structures, i.e., only the ferrite bar for core material and conducting wires. The other type is called the sensing coil type. The eddy currents on a no defect metallic surface yield the opposing magnetic fields to that of exciting currents. If there is a defect in the target metallic surface, then a part of the eddy currents has to take a detour path at the defect position and a flux is caused by this detour current. This flux is caught by an independently set coil. So that this type is called "sensing coil type".

Although a sensing coil type has higher sensibility than those of the impedance sensing type, the sensing coil type is composed of the somewhat complex structures, e.g., independent exciting and sensing coils are required.

Previously, we had exploited a highly sensitive sensing coil type sensor called the ∞ coil.

Principal purpose of this paper is to improve on this ∞ coil to the more high sensibility ECT sensor by considering the basic operating principles along with the intensive three dimensional finite element (3D FEM) simulations.

In our numerical simulations, we have assumed a line defect searching problem. So that our design target of the sensor is how to enhance the catching ability of the magnetic flux caused by the detouring eddy currents due to this line defect.

2 The ∞ coil

Figure 1 shows a typical planar type conventional ∞ coil which is composed of the two planar exciting coils and one sensing coil wound around the ferrite bar. According to the shape of the two exciting coils, we had named this sensor as "the ∞ coil" [3,4].

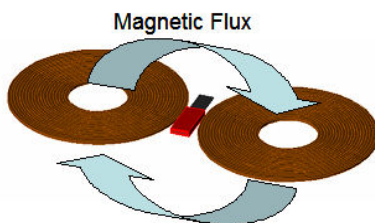


Figure 1. Schematic diagram of the ∞ coil, where the circular coils on both side are the planar exciting coils.

The red rectangular box is the sensing coil wound around a ferrite bar. The light blue arrows show the magnetic fluxes caused by the exciting currents.

2.1 Operating principle of the ∞ coil

When the alternating exciting currents flow through the exciting coils in an opposite direction, both two exciting coil construct the north and south magnetic poles, alternatively. Thereby, as shown in Figure 1, an exciting magnetic flux circulates through both of the two exciting coils.

Observe the exciting magnetic flux distributions shown in Figure 2 reveals that there is the no polarity zone, i.e., zero magnetic potential region between the two exciting coils. When we put on the ferromagnetic materials into this zero magnetic potential region, no magnetic field disturbance is occurred because of the zero magnetic potential. Thereby, it is possible to set the sensing coil wound around a ferrite bar in the zero magnetic potential region as shown in Figure 2.

Even if the exciting magnetic flux passes through this zero magnetic potential region, the surface of sensing coil is directed in parallel to this magnetic flux. So that, any voltage is not induced in the exciting coil.

If we put the ∞ coil on a no defect target metal surface, then the eddy currents flow as the image currents flowing in a opposite direction to the exciting currents. When there is no defect in a target object, the magnetic fields caused by the eddy currents never induce the voltage in the sensing coil. The reason why no induced voltage in the sensing coil is that any of the magnetic fields are directed in a parallel direction to the sensing coil surface.

However, if there is a defect in the target object, the detour eddy currents essentially flow along with the defect. Thus, the magnetic flux caused by these detour eddy currents induces a voltage in the sensing coil, and this induced voltage reveals the defect in the target object [5,6].

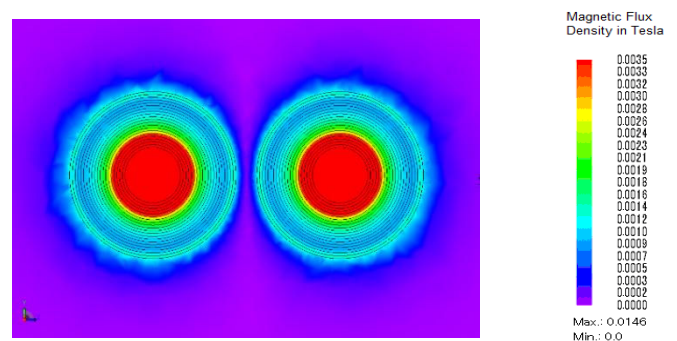


Figure 2. The magnetic flux density distributions caused by the ∞ coil (simulation).

2.2 Numerical Simulations

To verify the operation principle of the ∞ coil, we employ the 3D FEM simulations. Table.1 lists various constants used for the simulations.

Specification of the simulation model is as follows: A ∞ coil is

located in parallel to the copper test plate whose dimension is $100 \times 100 \times 1 \text{mm}^3$. A line defect is emulated by a $2 \times 60 \text{mm}^2$ slit, and this slit shape defect is set to 0, 45, 90 degrees to the sensing coil axis, 0.2mm lift-off distance. In addition to the Table.1, the 256kHz sinusoidal exciting current having 300mA(rms) amplitude is flowing thorough the two exciting coils.

Table 1. Various constants of the numerical simulations.

Exciting coil		Sensing coil	
Outer diameter	24.0 [mm]	Outer diameter	1.4×2.4 [mm]
Inner diameter	8.0 [mm]	Inner diameter	1.4×2.0 [mm]
Length	0.4 [mm]	Length	6 [mm]
Number of turns	20 turn	Number of turns	100 turn
Input voltage(peak)	1 [V]	Axis core	Mn-Zn/ferrite
Frequency	256 [kHz]		(Permeability: 3000)

Figure 3 shows the eddy current distributions on the target copper plate and the magnetic flux density distributions in the ferrite core.

Left of Fig. 3(a) shows the eddy current density distributions when no defect in the target copper plate. Right of Fig. 3(a) shows a flux density distribution in the ferrite core. The flux densities caused by the eddy currents are flowing along with the sensor coil surface in parallel. This means no induced voltage in the sensor coil when no defect in the target copper plate.

Left of Fig. 3(b) shows the eddy current distribution when a line defect is located in parallel to the sensor coil axis. The eddy currents flow along with this defect so that all of the magnetic flux caused by the eddy currents flow in a parallel direction to the sensor coil surface. Right of Fig.3(b) shows the flux density distributions in the ferrite core of the sensor coil.

Left of Fig. 3(c) shows the eddy current distributions when a line defect is located 45 degree to the sensor coil axis. The eddy currents flow along this line defect so that these eddy currents yield the perpendicular magnetic flux component to the sensor coil surface. Right of Fig. 3(c) shows the magnetic flux densities in the ferrite core directed 45 degree to the ferrite core axis. Thereby, the perpendicular magnetic flux component to the sensor coil surface induces the output voltage in the sensor coil.

Left of Fig. 3(d) shows the eddy current distributions flowing the detour paths to the defect when the line defect is located in a perpendicular direction to the sensor coil axis. Because of the flowing direction of the eddy currents, the magnetic flux flows in a perpendicular direction to the sensor coil surface. Although all of the magnetic flux caused by eddy currents are directed to the perpendicular to the sensor coil surface, they are cancelled each other. This means that it is difficult to

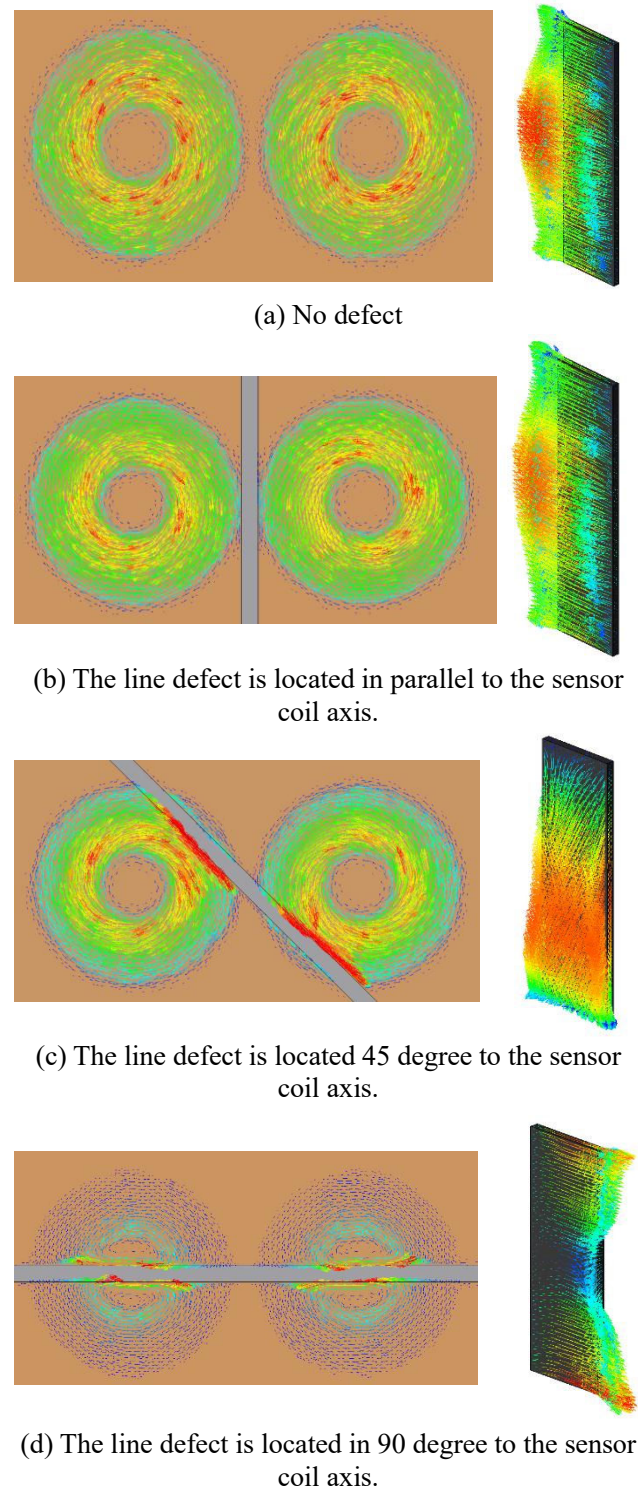


Figure 3. Eddy current distributions in various defect conditions and the magnetic flux density distributions in the ferrite core.

detect the line defect under this condition.

Figure 4 shows the induced voltage waveforms when the line defect is directed 0, 45, 90 degrees to the sensor coil axis. From the above results, it is found that the sensor coil could be induced the voltage when the detoured eddy current causes the perpendicular component of the magnetic flux to the sensor coil surface. The induced voltage in the sensor coil depends on the perpendicular magnetic flux component to the sensor coil surface so that the ∞ coil is one of the directional sensors.

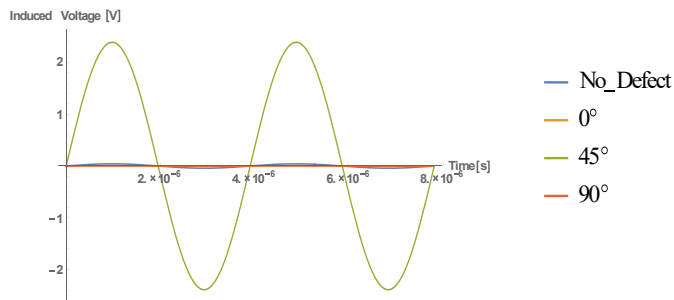


Figure 4 The induced voltages whose magnitude depends on the angle between the sensor coil axis and the magnetic flux flowing direction.

3 The planar semicircular shape ∞ coil

3.1 Key points

As described in Chapter 2, the operating principle is summarized into the two key points.

The first is that there is no polarity zone, i.e., zero magnetic potential region between the north and south poles when both of the north and south poles are constructed by the exciting coils.

When this zero magnetic potential region becomes a not zero magnetic potential, the defect is caught by the ∞ coil. This is a fundamental qualitative function of the ∞ coil, i.e. this is the same to the on/off function of a switch.

The second is that the magnetic flux is passing through no polarity zone, i.e., the zero magnetic potential region from the north to south poles. This magnetic flux is always directed in parallel to the sensor coil surface so that never induce the voltage in the sensor coil.

If the direction of this magnetic flux flow to the ferrite core axis is changed within 90 degree, then the changed angle is mostly proportional to the induced voltage in the sensor coil. In the other words, the directional change of the magnetic flux is the quantitatively function of the ∞ coil, i.e. the directional change within 90 degree is mostly proportional to the defect magnitude.

In this paper, we propose the exciting coils having the planar and semicircular shape to enlarge no polarity zone, i.e., the zero magnetic potential region between the north and south

poles. The two planar semicircular exciting coils construct the north and south poles alternatively by flowing the alternative exciting currents. A region between the two adjacent straight line of the two exciting coils constructs the line shape no polarity zone, i.e., zero magnetic potential region. The planar semicircular ∞ coil is composed of the two semicircular planar exciting coils and the sensing coil wound around a ferrite core as shown in Figure 5.

One of the big differences between the conventional and new ∞ coils is that no polarity zone, i.e., the zero magnetic potential region has been enlarged from the point in Figure 2 to the line in Figure 5.

As a result, it is possible to expect the higher sensibility of the new planar semicircular shape ∞ coil compared with those of conventional planar circular shape ∞ coil.

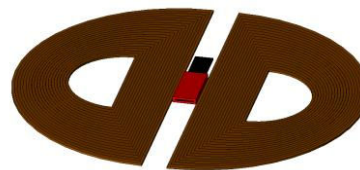


Figure 5. A planar semicircular ∞ coil

3.2 Numerical Simulations

To verify the operation of the new planar semicircular ∞ coil, we employ the 3D FEM simulations. Table.2 lists various constants of the exciting as well as the sensing coils.

Specification of the simulation model is as follows: The new planar semicircular ∞ coil is located in parallel to the copper test plate whose dimension is $100 \times 100 \times 1 \text{mm}^3$. A line defect is emulated by a $2 \times 60 \text{mm}^2$ slit, and this slit shape defect is set to 0, 45, 90 degrees to the sensing coil axis. 0.2mm lift-off distance. In addition to Table. 2, The 256kHz sinusoidal exciting current having 300mA(rms) is flowing thorough the two planar semicircular exciting coils.

Table. 2 Various constants of the planar semicircular ∞ coil.

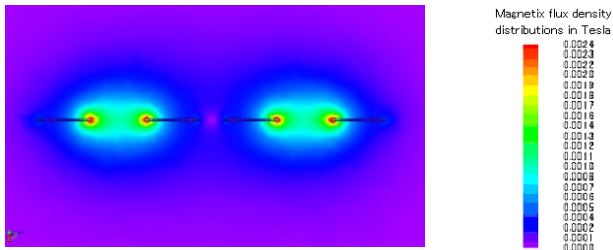
Exciting coil		Sensing coil	
Outer diameter	36.0 [mm]	Outer diameter	1.4×2.4 [mm]
Inner diameter	12.0 [mm]	Inner diameter	1.4×2.0 [mm]
Length	0.3 [mm]	Length	6 [mm]
Number of turns	20 turn	Number of turns	100 turn
Input voltage(peak)	1 [V]	Axis core	Mn-Zn/ferrite
Frequency	256 [kHz]		(Permeability: 3000)

Figure 6 shows the magnetic flux vector distribution and its magnitude by the simulations.

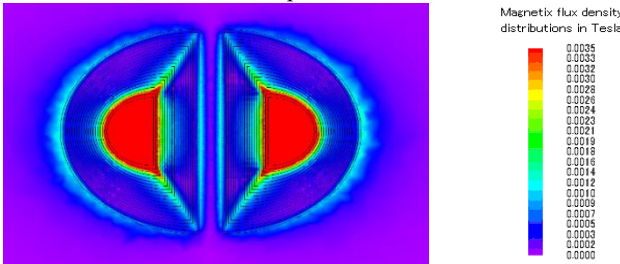
Figure 7 shows an induced voltage waveform when the line defect is directed 45 degree to the sensor coil axis. The new planar semicircular ∞ coil yields a higher sensor induced voltage compared with those of conventional one.

Also, the new semicircular ∞ coil yields a lower sensor induced voltage compared with those of conventional one when no detecting the defect.

The peak signal is the induced voltage at the 45 degree between the line defect and the sensor coil axis. The noise is defined the peak induced voltages at 0, 90, 180 degrees between the line defect and the sensor coil axis. This leads to the signal to noise, S/N, ratio definition. Comparison of this S/N ratio between the new planar semicircular ∞ and conventional ∞ coils suggests that the new planar semicircular ∞ coil proposed in this paper has a higher sensibility than those of conventional one.



(a) Cross-sectional view of the magnetic flux density vector distributions of the new planar semicircular ∞ coil.



(b) Plane view of the magnetic flux density vector distributions of the new planar semicircular ∞ coil.

Figure 6. The magnetic flux density vector distributions and its magnitudes of the new planar semicircular ∞ coil obtained by the simulations.

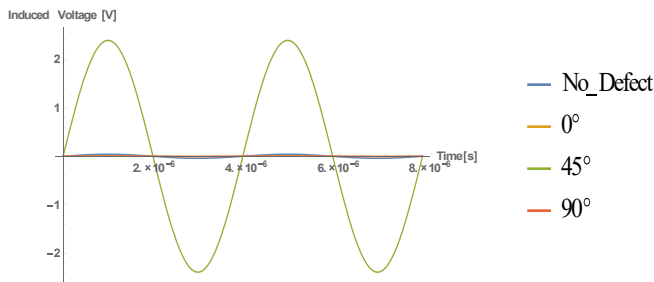


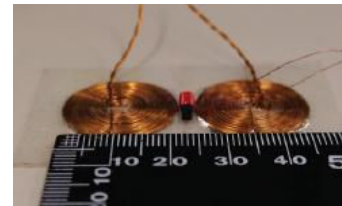
Figure 7. The induced voltages whose magnitude depend on the angle between the sensor coil axis and the magnetic flux flow direction in the sensing coil.

The experimented and simulated S/N ratios are compared in order to check up the validity of simulations.

The tested copper plate has a $1 \times 1 \text{mm}^2$ line defect. Table.3 lists various constants of the tested ∞ coils. The peak sinusoidal excitation voltage was 1V and 256kHz.

Table.3 Various constants of the tested ∞ coils

(a) circular exciting coil	(b) semicircular exciting coil	(c) sensing coil
Coil outer diameter 9.0 [mm]	Coil outer diameter 18 [mm]	Outer diameter 1.4×2.4 [mm]
Coil Inner diameter 0.5 [mm]	Coil Inner diameter 1 [mm]	Inner diameter 1.0×2.0 [mm]
Coil length 0.3 [mm]	Coil length 0.3 [mm]	Length 6 [mm]
Number of turns 20	Number of turns 20	Number of turns 100
Input voltage (peak) 1 [V]	Input voltage (peak) 1 [V]	Axis core Mn-Zn /ferrite
Frequency 256 kHz	Frequency 256 kHz	(permeability:3000)



(a) Planar circular exciting ∞ coil



(b) Planar semicircular exciting ∞ coil



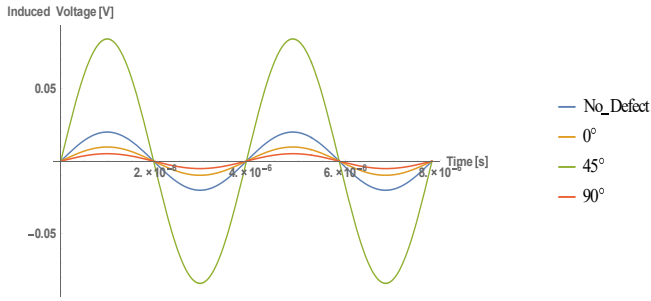
(c) Sensing coil

Figure 8. The pictures of tested ∞ coils, where the upper, middle and lower are the conventional ∞ coil, the new planar semicircular ∞ coil and sensing coils wound around a ferrite bar, respectively.

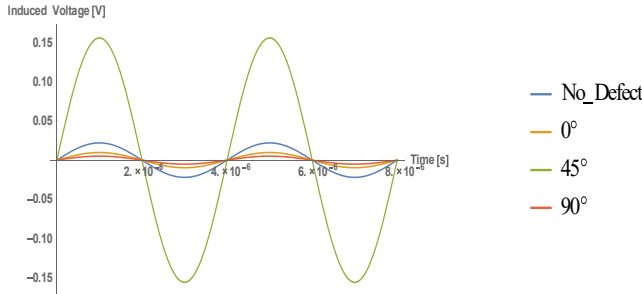
Figure 9 shows the experimentally obtained signal voltage waveforms of the conventional as well as new planar semicircular ∞ coils.

Table 3 summarizes the simulated and experimented results of both conventional and new planar semicircular ∞ coils.

Thus, it is clarified that the new semicircular ∞ coil yields a higher sensor sensibility compared with those of conventional one.



(a) Conventional ∞ coil



(b) New planar semicircular ∞ coil

Figure 9. Comparison among the experimentally obtained sensor signal waveforms of the conventional as well as new planar semicircular ∞ coils.

Table.3 The S/N ratios

	Conventional ∞ coil		New semicircular ∞ coil	
	Simulation	Experiment	Simulation	Experiment
No defect	0.006V _{peak}	0.020V _{peak}	0.0014V _{peak}	0.022V _{peak}
45°	0.100V _{peak}	0.084V _{peak}	0.1599V _{peak}	0.156V _{peak}
S/N ratio	16.67	4.20	114.21	7.09

Because of the skillfulness to work out the practical coils, the large differences between the simulated and experimented results in both of the conventional and new planar semicircular ∞ coils could be found in Table 3.

The differences between the conventional and its experimented values are smaller than that of the new planar ∞ coil. This is because the geometrical shape is much more serious parameter to work out the practical planar ∞ semicircular coil.

4 Conclusion

As shown above, we have proposed the new semicircular ∞ coil in the present paper. Employment of the two planar semicircular exciting coils has made it possible to enlarge the zero magnetic potential region. Thereby, it has been possible to enhance the sensibility of the ∞ coil.

In addition, the results of the 3D FEM simulation and of the practical experiments have verified that the newly developed semicircular ∞ coil yields the higher S/N ratio than that of conventional one.

REFERENCES

- [1] Narishige, S., Nishimizu, A., Koike, M., Abe, M., Narumi, Y., Tsuge, T. (2010), Improved Detection Performance using a Multi-frequency Method of Eddy Current Testing for Outside Circumferential Cracks near an Expansion of Heat Exchanger Tubes, Non-Destructive Testing and Condition Monitoring, Vol. 52(6), June 2010, pp. 298-301.
- [2] Hashizume, H., Yamada, Y., Miya, K., Toda, S., Morimoto, K., Araki, Y., Satake, K. and Shimizu, N., (1992), Numerical and Experimental Analysis of Eddy Current Testing for a Tube with Cracks, 1992, Vol.28, pp.1469 - 1472.
- [3] Morozov, M., Rubinacci, G., Tamburrino, A. and Ventre, S., (2006), Numerical Models of Volumetric Insulating Cracks in Eddy-Current Testing with Experimental Validation, IEEE Trans. Magn. 2006, Vol.42, pp.1568 - 1576.
- [4] Kikuchihara, H. and Saito, Y., (2013), Enhance the Sensibility of the ECT Sensor, Journal of the Japan Society of Applied Electromagnetics and Mechanics, Vol.21(3), 2013.
- [5] Maruyama, K., Marinova, I., and Saito, Y., (2014), Enhance the Sensibility of the Resonance type ECT Sensor, Materials Science Forum Vol. 792, 2014, pp 72 - 77.
- [6] Maruyama, K., Marinova, I., and Saito, Y., (2015), Developments of Flat ∞ Coil for Defect Searching in the Curved Surfaces, E-Journal of Advanced Maintenance, (EJAM), Vol.7-1, 2015, pp. 59-65.

Contact

takahiro.hyuga.8k@stu.hosei.ac.jp

E-mail

Address:

Ingenious Resonance Circuit Connection for Resonance Type Eddy Current Sensors

Kazuya OKUDA and Yoshifuru SAITO

Hosei University, Graduate School of Electrical and Electronic Engineering,
3-7-2 Kajino-cho, Koganei-shi, Tokyo 184-8684, Japan

Abstract

This paper describes the resonant connection for constructing a resonant circuit without any external capacitor. Resonance connection is an ingenious circuit connection which makes it possible to utilize the line to line capacitor and inductance for resonance not requiring any additional external capacitors.

In the present paper, the resonant frequency of ingeniously connected circuits could be controlled by changing the twist pitch of two coils. Further, this resonant connection is applied to a resonant type eddy current sensor. As a result, it is revealed that our new resonant type eddy current sensor has higher sensibility compared with those of conventional eddy current sensor.

Keyword: Ingenious resonant coils connection, Eddy current testing, Nondestructive testing

1 INTRODUCTION

Various non-destructive testing methods, such as eddy current testing (ECT), ultrasonic testing (UT), radiographic testing (RT) and acoustic emission (AE) are currently used to the modern airplane, high-speed train and express highway bus maintenance. Among these methods, ECT does not require the complex electronic circuits, and does not need direct contact to the tested specimens.

To overcome the various difficulties caused by the ferromagnetic material properties as well as surface deformation of the tested specimen, a multi-frequency drive ECT probe had been proposed. As a result, several fruitful results had been reported for the tests of tube with cracks [1]. Also, numerical and experimental analysis of eddy current testing for a tube with cracks had been carried with satisfactory results. [2,3]

Operating principle of the ECT is classified into the two major categories. One is that exposing the conductive materials to the alternating magnetic fields induces eddy current in all of the conducting materials. Thereby, the input impedance of the magnetic field source, i.e., electric source, can detect the change of the target impedance caused by defects blocking eddy current flowing. The ECT based on this principle is called impedance sensing type.

The other type utilizes a separately installed sensor coil to detect the leakage magnetic flux change. The magnetic field of ECT is composed of two components: one is the exciting and the other is the reactive component of magnetic fields. The reactive component of magnetic field is caused by the eddy currents in

the target so that change of eddy current paths changes the reactive magnetic fields. Thus, the independently installed sensor detects this magnetic field change. This type is called a separately sensing coil type. In the other words, operating principle of the separately installed sensing coil type ECT is as follows: the sensing coil catches the magnetic field intensity variation caused by the detour eddy currents flowing around a defect in the target metallic materials. [4-6].

The impedance sensing type is further classified into two types. One is a simple impedance detecting type and the other is the resonant impedance detecting type. So that this latter type is called the resonance type ECT.

Previously, an ingenious coil connection exhibits a single resonant frequency characteristics has been applied to work out the noise filter for the power electronics circuits [4]. Further, this ingenious coil connection has been applied to the resonance type ECT [5]. Even though, the resonance type ECT utilizing the ingenious coil connection exhibits higher sensibility compared with those of a conventional ECT, the operating frequency of the resonance type ECT is so high that it has been forced to attach an external capacitor to reduce the resonance frequency [6].

In the present paper, the resonant frequency of ingeniously connected circuits could be controlled by changing the twist pitch of two coils with the aid of ferromagnetic core materials. As a result, it is revealed that our developed new resonant type ECT has higher sensibility compared with those of conventional impedance detecting type ECT sensor.

2 RESONANT TYPE ECT

2.1 Fundamentals

Let an arbitrary finite length solenoid coil shown in Fig. 1(a) be an eddy current sensor coil. When we put this sensor coil on a copper plate as shown in Fig. 1(b) and apply an alternating current to the sensor coil, eddy current is induced as a reaction of the alternating magnetic fields because of the Faraday's law. Measure the input impedance of the sensor coil is able to diagnose a difference of the target copper plate condition between no defects (Fig. 1(b)) and 2mm crack defect (Fig. 1(c)). This is similar to the secondary impedance change detection from primary input terminal in a conventional single phase transformer. Thus, it is obvious that a simple finite length solenoid coil can detect the defects of the target conducting materials. This is the basic operating principle of the impedance sensing type ECT.

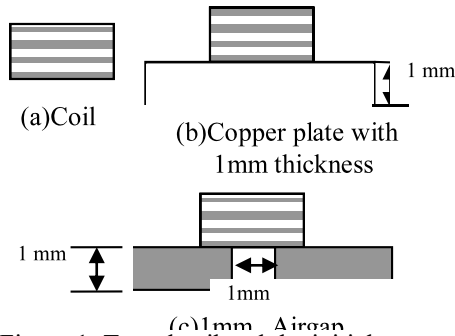
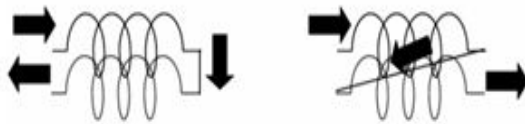


Figure 1. Tested coil and the initial measurement conditions.

2.2 Resonant Type ECT

Any of the coils always exhibit an inductive property because of the magnetic fields around them when applying a current into the coil. Also, any of the coils have the capacitances among the coils. Even though a simple finite length solenoid coil shown in Fig. 1(a), it is possible to observe its natural resonance phenomena as shown in Fig. 3.



(a) Normal. (b) Ingeniously connection.

Figure 2. Constructions of the finite lengths solenoid coils. (a) Normal and (b) ingeniously connected conducting wires.

Figure 3 shows that the normal in Fig. 2(a) and the ingeniously

connection in Fig. 2(b) of the conducting wires are constructing the normal and the ingeniously connected finite length solenoid coils, respectively.

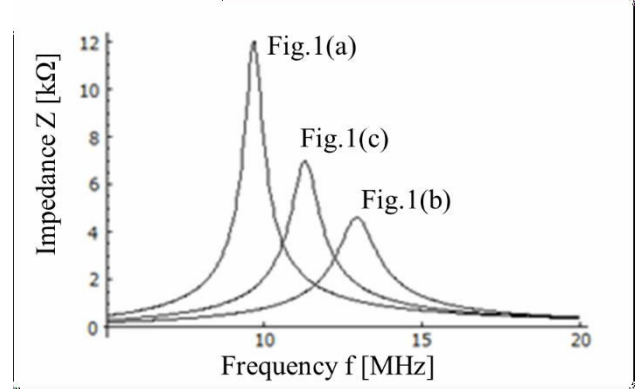


Figure 3. Frequency characteristics of the impedances of the finite length coil shown in Fig. 1(a), on the copper plate with 1mm thickness shown in Fig. 1(b) and on the two discrete copper plates shown in Fig. 1(c).

Decision of ECT operation frequency is of paramount importance, because sensibility and searching depth of ECT are greatly depending on the operation frequency. Theoretically, the operation frequency of ECT can be decided by taking the target conductivity and its skin-depth into account. However, final selection of operation frequency is determined by the past experiences and the practical tests.

In this paper, the operation frequency of ECT has been set to the natural parallel resonant frequency of the ECT sensor coil when facing with a wholesome part of target. The ECT facing with the wholesome part of target takes the maximum pure resistive impedance. When the ECT sensor coil meets with a defect of target, the resonance condition is essentially not established. Therefore, the input impedance of the input terminals is also reduced to small in value compared with those of the resonant one. Namely, a deviation between the resonance and not resonance impedances becomes the maximum value.

A sensibility ε of ECT is defined by

$$\varepsilon = \frac{|reference - measured|}{reference} \times 100 [\%] \quad (1)$$

where the reference and measured in (1) refer to the input impedances from the ECT coil terminals when facing the ECT coil with the wholesome and defect parts of target, respectively.

INGENIOUS COIL CONNECTIONS

3.1 Resonant frequency control

Stray capacitance control makes it possible to govern the natural resonance phenomena. The ingenious coil connection in Fig. 4 is one of the control methods of the stray capacitances among the coils.

Twisting of the two coils in Fig. 5 is not only the facing between the black and white coils into uniform but also it is possible to control the resonant frequency.

We had worked out the 13 twisted coils by changing the twist pitch as well as a number of layers. A coil diameter of the 13 twisted coils is 0.2mm.

Table 1 list the various constants of the 13 twist coils.

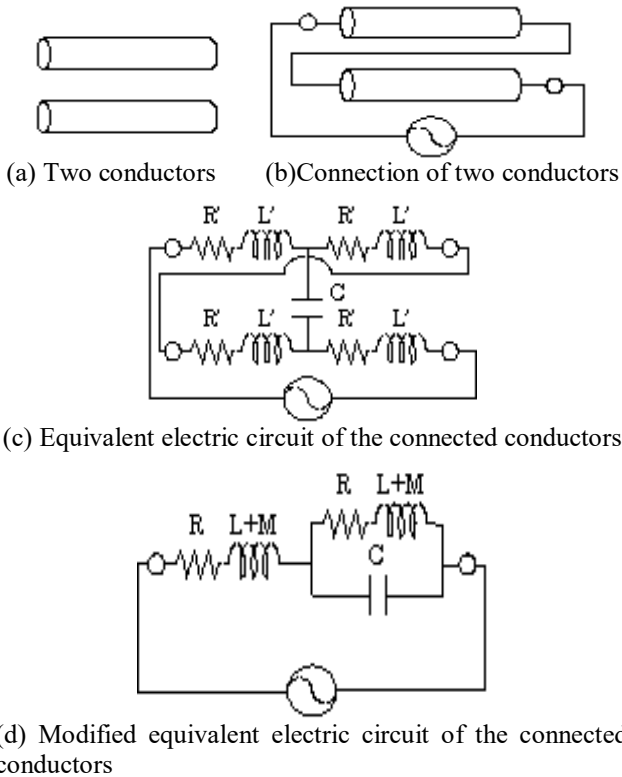


Figure. 4. Principle of an ingenious coil connection.

The most important key point to realize the ingenious connection is to twist the coils as shown in Fig. 5. Twisting of the coils makes it possible to control the resonant frequency due to the stray capacitance between two coils.

Measuring the defect or no defect resonant impedances extracts a shape of defect. Figure 6 shows an example of an extracted H shape defect.



Figure. 5. Example of a pair of twisted coils

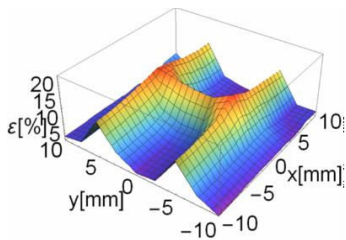


Figure.6. Extracted H shape defect by measuring the resonance impedances..

3 RESONANT TYPE ETC UTILIZING THE

Twist pitch [turn/m]	Number of layer [layer]	Resonant frequency [kHz]
1470.6	1	309.0
1250.0	1	481.5
500.0	1	543.0
333.3	1	580.5
200.0	1	570.0
142.9	1	679.5
1470.6	2	233.5
500.0	2	173.0
333.3	2	181.5
200.0	2	180.0
142.9	2	252.5
1470.6	3	194.0
333.3	3	196.0

Figures 7 shows the frequency vs. impedance characteristics of the twist coils when changing the twist pitch as well as the number of layers.

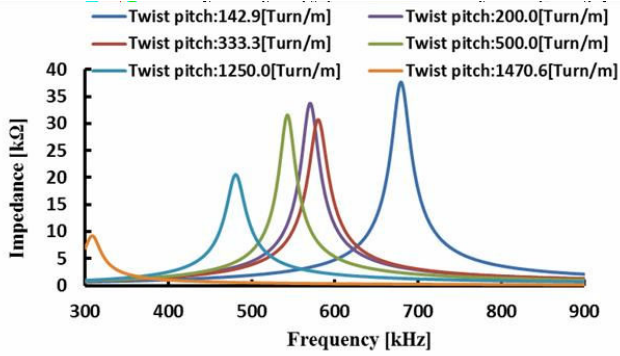
Observe the impedance vs. frequency characteristics of the single layer coils in Fig. 7 reveals that increasing of the twist pitch decreases the resonant frequency. However, it is found that increasing the number of layers decreases the effects of twist pitch as shown in the Figs. 7(b)-(c).

To represent a relationship among the resonant frequency, twist pitch and number of layers, we have derived an empirical formula by a least squares.

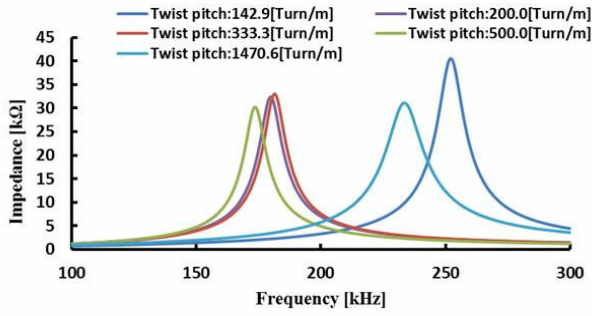
Let us consider the x,y,z coordinate system, where the coordinate values x,y,z are corresponding to the twist pitch, number of layers and resonant frequency, respectively.

To represent a relationship among the twist pitch x , number of layers y and resonant frequency z , let us consider an empirical formula given by

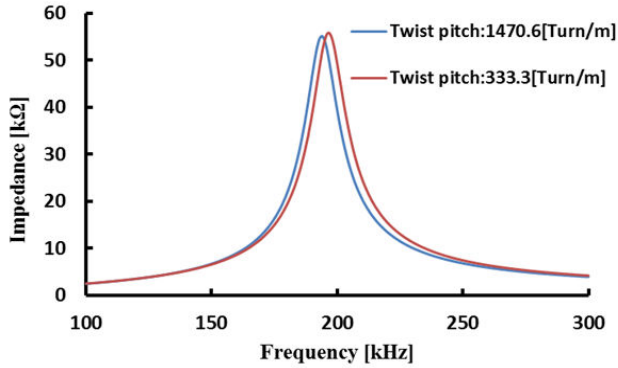
$$f = c_0 + a_1x + b_1y + a_2x^2 + b_2y^2 + c_{11}xy + a_3x^3 + c_{12}xy^2 + c_{21}x^2y \dots \quad (2)$$



(a) Single layer



(b) Double layers



(c) Triple layers

Figure. 7. The frequency vs. impedance characteristics of the twist coils when changing the twist pitch as well as layers.

We have $m=13$ equations and $n=6$ unknowns of (2) so that the least squares of (3) gives 6 unknowns. Thus, we have the empirical formula (4).

As shown in Fig. 8, this empirical formula yields a set of design curves for the ingenious resonant connection circuits, i.e., a resonant frequency is represented as the functions of the twist pitch as well as number of layers.

$$\begin{bmatrix} f_1 \\ f_2 \\ f_3 \\ f_4 \\ \vdots \\ f_m \end{bmatrix} = \begin{bmatrix} 1 & x_1 & y_1 & \dots & \nu_1 \\ 1 & x_2 & y_2 & \dots & \nu_2 \\ 1 & x_3 & y_3 & \dots & \nu_3 \\ 1 & x_4 & y_4 & \dots & \nu_4 \\ \vdots & \vdots & \vdots & \ddots & \vdots \\ 1 & x_m & y_m & \dots & \nu_m \end{bmatrix} \begin{bmatrix} c_0 \\ a_1 \\ b_1 \\ \vdots \end{bmatrix} \quad (3)$$

$$m \gg n,$$

$$\mathbf{y} = \mathbf{C} \cdot \mathbf{x},$$

$$\mathbf{x} = (\mathbf{C}^T \mathbf{C})^{-1} \mathbf{C}^T \mathbf{y},$$

where \mathbf{C} and \mathbf{C}^T are the system matrix and its transpose, respectively

$$f = 1367.94 - 0.33453x + 0.0000283815x^2 - 874.771y + 0.116112xy + 156.323y^2 \quad (4)$$

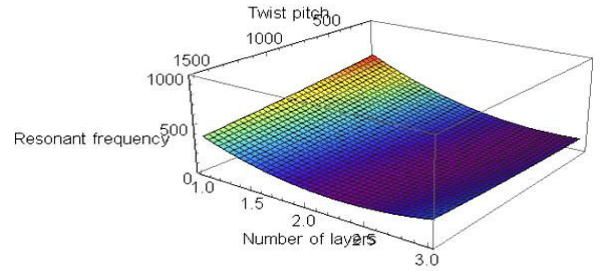


Figure 8. Design curves for the ingenious connection resonant circuit, where a resonant frequency is given as a function of the twist pitch as well as number of layers.

Even though the coil diameter is limited to 0.2mm, a desired resonance frequency decides the twist pitch and number of layers from the design curves in Fig. 8.


Thus, our empirical formula approach makes it possible to control the resonant frequency without any external capacitor.

3.2 Flaw detection

To demonstrate the usefulness of our resonance type ETC utilizing the ingenious coil connections, we have carried out a flaw detection in a two-dimensional plane.

Figure 9 is the target test piece having an artificial defects of width 2mm and depth 1mm.

Table.2 Prototype ECT sensor

	Length of entire coil	2260mm
	Coil diameter	0.1mm
	Number of turns	120turns
	Length of solenoid coil	30mm
	Number of layer	1

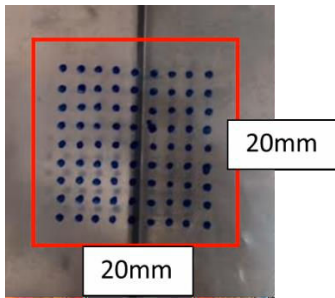


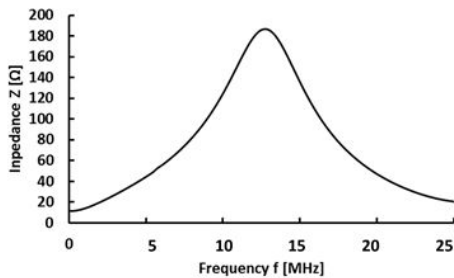
Figure 9. Tested target metal sheet having the width 2mm and depth 1mm artificial defect. Black dots denote the measured points.

At first, we have designed our prototype of the resonant connection type ECT coils by the empirical formula (4). Second, a ferromagnetic material whose diameter of 6 mm, length of 30 mm is employed to control the resonance frequency in a much more precisely.

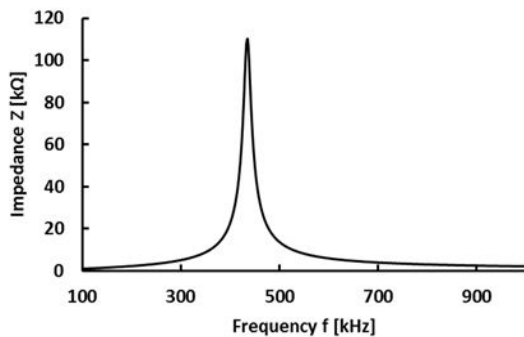
Table 2 lists various constants of an exploited resonance connection type ETC employing the ingenious coil connections with a ferrite rod.

Figure 10(a) shows an impedance versus frequency of a normal finite length solenoid coils without any ingenious connection.

Figure 10(b) shows an impedance versus frequency of the resonant connection type coils.



(a) Normal finite length solenoid coil



(b) Resonant connection type coil

Figure 10. The impedance versus frequency characteristics of the coils.

A red square in Figure 9 shows a 20mm by 20mm target area

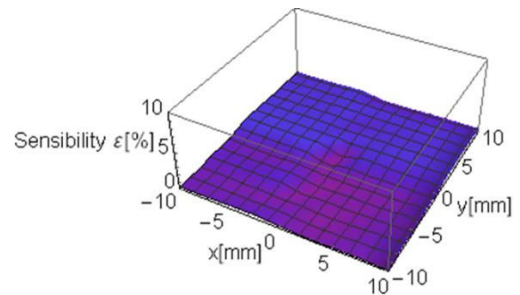
for ECT. The ECT sensors measured at the 9 by 9 sampling points with 2.5mm regular spacing on this 20mm by 20mm square area.

A driving frequency of both the normal finite length coil in Figure 10(a) and the resonant connection type coils in Figure 10(b) has been set to 256kHz.

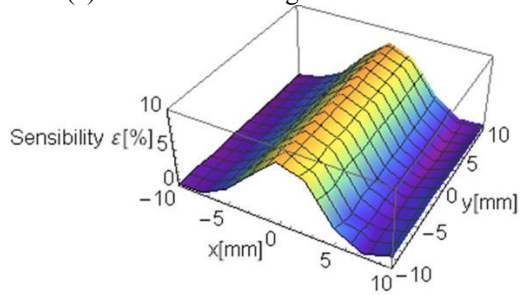
Setting the reference point at a lower left corner in Figure 9 gives the sensibilities of (1).

Figure 11(a) shows a sensibility distribution of the normal finite length solenoid coil.

Figure 11(b) shows a sensibility distribution of the resonance connection type coils.



(a) Normal finite length solenoid coil



(b) Resonant connection type coil

Figure. 11. Sensibility of (1) distributions of the normal finite length solenoid coil and the resonant connection type coil..

The sensibility distributions in Figure 11 reveals that the resonant type coil yields a far excellent sensibility compared with those of the normal finite length solenoid coil.

In the other words, nearer the exciting frequency is the resonant frequency of the sensor coil, the more high sensibility the sensor coil exhibits.

To confirm this, we have carried out an experiment a resonance connection type coil installed around a ferrite bar.

Figure 12 shows an impedance versus frequency of the resonant connection type coils installed to the ferrite rod. Obviously, the resonant frequency of this coil is nearer to the exciting frequency 256KHz.

Figure 13 shows a sensibility distribution of the resonance connection type coils installed to the ferrite rod..

Thus, we have succeeded in exploiting the new resonance type

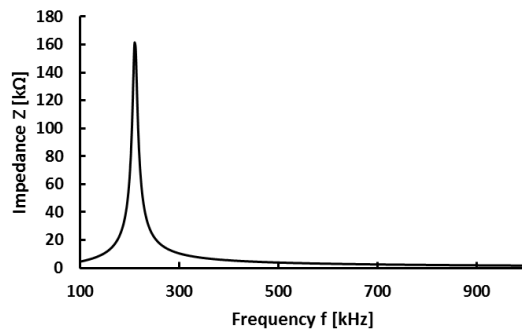


Figure 12. A frequency versus impedance characteristics of the resonance connection type coil installed to a ferrite rod.

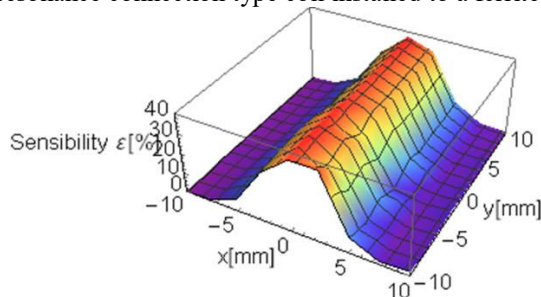


Figure 13. Sensibility distribution of the resonance connection type coil installed to a ferrite rod..

ECT sensor having high sensibility.

A most important key point is that nearer the exciting frequency is the resonant frequency of the sensor coil, the more high sensibility the sensor coil exhibits.

4 CONCLUSION

This paper has been described to the improvement of the resonant type ECT.

Previously, we had proposed an eddy current sensor of new resonance type by an ingenious coil connection.

Even though this new resonance type ECT sensor does not need any external capacitor to maintain a stable resonance state and has a very high sensitivity, consideration of the skin depth has lead to employ a lower operating frequency.

To overcome this resonant frequency control, this paper proposes an empirical formula based of the least squares. As a result, we have succeeded in designing the resonance type ECT without any external capacitor.

REFERENCES

- [1] S.Narishige, A.Nishimizu, M.Koike, Y.Abe, Y.Narumi, T.Tsuge, Improved Detection Performance using a Multi-frequency Method of Eddy Current Testing for Outside Circumferential Cracks near an Expansion of Heat Exchanger Tubes, Non-Destructive Testing and Condition Monitoring, Volume 52, Number 6, pp.298-301, June 2010.
- [2] H.Hashizume, Y.Yamada; K.Miya, S.Toda, K.Morimoto, Y.Araki, K.Satake, N.Shimizu, Numerical and Experimental Analysis of Eddy Current Testing for a Tube with Cracks. IEEE Trans. Magn. 28, pp.1469-1472, 1992,.
- [3] M.Morozov, G.Rubinacci, A.Tamburrino, S.Ventre, Numerical Models of Volumetric Insulating Cracks in Eddy-Current Testing with Experimental Validation, IEEE Trans. Magn. 42, pp.1568-1576, 2006.
- [4] Y.Midorikawa, S.Hayano and Y.Saito, A resonant phenomenon between adjacent series connected coils and its application to a noise filter, Advanced Computational and Design Techniques in Applied Electromagnetic Systems, Vol.6, pp. 633-639, 1995.
- [5] H. Kikuchihara, I. Marinova and Y. Saito, Enhance the Sensibility of the Eddy Current Testing, Journal of the Japan Society of Applied Electromagnetics and Mechanics, Vol. 21, No. 5, pp.356-361, 2013.
- [6] K. Maruyama, I. Marinova and Y. Saito, Enhance the Sensibility of the Resonance Type Eddy Current Testing, Materials Science Forum Vol. 792, pp.72-77, 2014.

Contact E-mail Address: kazuya.okuda.2n@stu.hosei.ac.jp